ORIGINAL ARTICLE

Automated machine tool dynamics identification for predicting milling stability charts in industrial applications

Vahid Ostad Ali Akbari[1] · **Christian Schuppisser**[1] · **Michal Kuffa**[1] · **Konrad Wegener**[1]

Abstract

As the machine tool dynamics at the tooltip is a crucial input for chatter prediction, obtaining these dynamics for industrial applications is neither feasible through experimental impact testing for numerous tool-holder-spindle combinations nor feasible through physics-based modeling of the entire machine tool due to their sophisticated complexities and calibrations. Hence, the often-chosen path is a mathematical coupling of experimentally measured machine tool dynamics to model-predicted tool-holder dynamics. This paper introduces a novel measurement device for the experimental characterization of machine tool dynamics. The device can be simply mounted to the spindle flange to automatically capture the corresponding dynamics at the machine tool side, eliminating the need for expertise and time-consuming setup efforts thus presenting a viable solution for industries. The effectiveness of this method is evaluated against conventional spindle receptance measurement attempts using impact tests. The obtained results are further validated in the prediction of tooltip dynamics and stability boundaries.

Keywords Chatter stability · Machine tool dynamics · Piezoelectric actuators · Structural coupling · Inverse RCSA

1 Introduction

Until today, regenerative chatter has been the main factor limiting the productivity of milling operations in manufacturing industries. Despite the extensive research on this topic since its first attention by Tlusty and Polacek [1] in 1963, a solid solution implementable in an industrial environment is still lacking.

While stability lobe diagrams (SLDs) provide a powerful solution to predict the boundary between stable and unstable axial depth of cut as a function of spindle speed [2], they are barely used in industries due to the significant measurement and modeling effort that is required for their creation.

An existing SLD allows for a proper selection of depth of cut and spindle speed leading to a significant productivity increase while chatter and its negative consequences are prevented. However, a blind selection of process parameters may lead to poor surface quality, significant tool wear, damage to the machine tools, increased production cost, and excessive noise emissions.

Regardless of the stability models being formulated in frequency [2–4] or time domain [5, 6], the generation of SLDs requires precise knowledge of cutting forces and the dynamics at the tip of end mills, where the cutting forces excite the machine tool structure. While the cutting forces can be characterized by simplified coefficients [2], the complexity of obtaining machine tool dynamics has remained the major obstacle in industrial profits from SLD predictions. It is worth noting that the knowledge of system dynamics is not merely useful in SLD creation, but also essential for control applications, where the interaction between mechanical and mechatronic subsystems determines the performance of machine tool controllers [7, 8]. Further insights into applications of machine dynamics can be found in [9].

Modeling the entire machine tool structure including the tool-holder assembly is challenging, due to missing information (such as the bearing locations) and the unknown damping characteristics of the numerous joints of the machine tool structure [10, 11]. Hence, a direct experimental measurement of the tooltip dynamics using impact hammers may seem an immediate option. While direct measurement of tooltip dynamics can be used for the generation of a precise SLD, it can be very time-consuming and prone to errors due to inaccurate impact location and direction during manual tap testing. This conventional measurement approach typically

✉ Vahid Ostad Ali Akbari
  oaavahid@iwf.mavt.ethz.ch

1 Institute of Machine Tools and Manufacturing (IWF),
  ETH Zürich, Zürich, Switzerland

has a drawback that the measurements need to be repeated for every tool-holder combination used on a shop floor which makes the number of required experiments grow exponentially as the number of machines, tool holders, and tools increases.

An alternative and commonly used path is to combine the experimentally measured dynamics of the machine tool substructure with the analytically modeled dynamics of the tool-holder combination through receptance coupling substructure analysis (RCSA) [12]. This is a promising approach since analytical tool-holder models using Timoshenko beam elements accurately model the dynamics of tool-holder assemblies [13].

Researchers have explored various methods for identifying machine dynamics. One approach involves analyzing cutting forces as a source of excitation and using resulting vibrations to estimate the underlying dynamics [14, 15]. Alternatively, some researchers have relied on impact testing with a dummy cylindrical object mounted to the spindle interface. This approach, known as inverse RCSA, allows for the mathematical subtraction of the dummy cylinder to obtain the dynamics [2, 16, 17]. The approach alleviates the challenges of exciting rotational DOFs and measuring their responses directly. Even in sophisticated studies that combine machine learning with mathematical models [18, 19], it is often assumed that the machine tool's dynamics are known from the inverse RCSA method. However, it is important to note that this approach can be demanding in terms of conducting a large number of impact tests, especially if capturing the position-dependent machine dynamics across different positions in the workspace is the goal [20] or when dealing with numerous machine tools in real manufacturing companies.

This paper presents an industry-friendly and accurate identification method for the experimental measurement of machine tool dynamics to automate the characterization of the machine tool dynamics at the spindle interface.

The proposed measurement devices are designed to be easily mountable to a machine tool's spindle interface analogous to a tool holder. Multiple piezoelectric actuators are embedded into the device structure that enable the excitation of the spindle structure by applying alternating voltage, replicating a similar concept as an inertial shaker. Simultaneously, integrated accelerometer sensors monitor the system response at multiple locations leading to the collection of sufficient information for the estimation of translational and rotational dynamics of the machine tool at its spindle flange. Compared to other existing automated hammer designs [21] that need external support and precise adjustments to align accurately with the intended direction of the excitation force, this design incorporates actuators and essential sensors into a singular unit, allowing for easy installation into the machine tool interface, thereby enhancing its practical feasibility for

industrial applications. It also allows the spindle to travel through the workspace to capture potential position dependencies of the machine tool dynamics. In the end, this device eliminates the need for hammer impacts and can be used at the end of the assembly line in machine tool manufacturing companies to characterize the machine tool dynamics and provide their customers with this pivotal information.

The remainder of this paper is structured as follows: in Section 2, two prototype designs of the spindle receptance identification device are described along with suitable reconstruction methods. Section 3 presents different methods for acquiring dynamics models of individual devices. Section 4 investigates the validation of reconstructed spindle dynamics versus other methods from the literature, dynamics at the tooltip, and prediction of stability boundaries. Finally, the paper is concluded in Section 5.

2 Methodology

This section outlines the underlying operational concept of the proposed automatic devices. Section 2.2 introduces the substructure coupling concept, shedding light on the mathematical feasibility of automatic reconstruction methods. Building upon these foundations, it delves into the design concept and the methods for reconstructing the spindle's dynamics in the two distinct layouts of the device, which are detailed in Sections 2.2.1 and 2.2.2.

2.1 Multi-component structural coupling concept

The presented approach consists of a measurement device with integrated piezoelectric actuators and accelerometers which is mounted to a machine tool spindle through a standard tool-holder interface (e.g., HSK A63). The embedded actuators excite the device and the connected machine tool structure with the embedded sensors recording the response of the coupled structure. Finally, the dynamics of the machine tool without the device are retrieved by mathematically decoupling the known device dynamics. Figure 1 illustrates the conceptual coupling of a generic non-rigid structure representing the device, denoted as substructure D, and the structure of machine tool and spindle, denoted as substructure S. The resulting assembly of the machine tool structure and device is denoted as structure A.

Capital variables denote frequency domain quantities whose dependency on frequency $s = j\omega$ is omitted from the notation for simplicity in the remainder of this document. Furthermore, variables in bold denote non-scalar quantities, i.e., vectors or matrices.
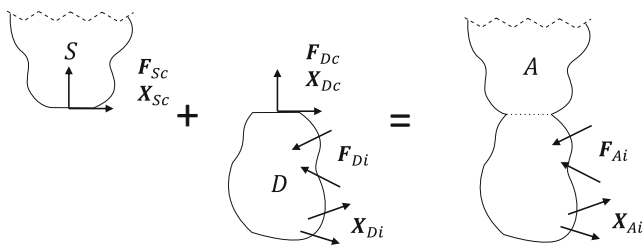
Fig. 1 Generic structural coupling scheme of the measurement device and spindle. The receptance coupling allows relating the dynamics of the assembly to the dynamics of its components

Let $H_{S,cc}$ denote the spindle receptance matrix which relates frequency domain forces $F_{S,c}$ to frequency domain displacements $X_{S,c}$ at the spindle interface:

$$X_{S,c} = H_{S,cc} F_{S,c} \tag{1}$$

The subscript c indicates that the corresponding degrees of freedom (DOFs) to the forces and displacements participate in the coupling as will become more obvious once the device receptance has been presented. Axial and torsional dynamics of the spindle are usually neglected in the context of chatter prediction in milling operations and the spindle receptance matrix remains confined to bending dynamics in a four-by-four matrix relating the force vector $F_{S,c} = [F_x, F_y, M_x, M_y]^T$ to the displacement vector $X_{S,c} = [X, Y, \theta_x, \theta_y]^T$. In this work, axis cross-coupling components of the spindle dynamics are neglected, as they are roughly an order of magnitude smaller on common machine tool structures compared to in-axis components. This simplifies the formulations to uni-directional cases, i.e., $X_{S,c} = [X, \theta_x]^T$ and $F_{S,c} = [F_x, M_x]^T$ (and analogous for the Y direction). The presented equations hold also for the more general case including axis cross-coupling terms.

Let H_D denote the device receptance matrix. The relevant DOFs of the device are divided into two groups: a group of DOFs that will be coupled with the spindle (subscript c) and a group of DOFs which will remain independent (subscript i). The uncoupled dynamic response of substructure D can then be described by the following:

$$\begin{bmatrix} X_{D,c} \\ X_{D,i} \end{bmatrix} = H_D \begin{bmatrix} F_{D,c} \\ F_{D,i} \end{bmatrix}, \text{ where } H_D = \begin{bmatrix} H_{D,cc} & H_{D,ci} \\ H_{D,ic} & H_{D,ii} \end{bmatrix} \tag{2}$$

Here, $X_{D,c}$ and $X_{D,i}$ are vectors of frequency domain displacements at coupled and independent coordinates, respectively. Analogously, $F_{D,c}$ and $F_{D,i}$ are vectors of frequency domain forces at coupled and independent DOFs, respectively. The detailed derivation of the device model is presented in Section 3.

Furthermore, let $H_{A,ii}$ be the dynamics of the rigidly coupled system A, as illustrated in Fig. 1, such that

$$X_{A,i} = H_{A,ii} F_{A,i} \tag{3}$$

The rigid coupling of substructures D and S is enforced by the compatibility and equilibrium conditions of $X_{D,c} = X_{S,c}$ and $F_{D,c} + F_{S,c} = 0$, respectively. As a result, $H_{A,ii}$ can be expressed in terms of its substructure receptances through linear receptance coupling [22]:

$$H_{A,ii} = H_{D,ii} - H_{D,ic}(H_{D,cc} + H_{S,cc})^{-1} H_{D,ci} \tag{4}$$

The device dynamics H_D can be obtained through a calibrated model of the device's structure. The dynamics of the coupled structure A is computed from the experimental measurements by the device when it is mounted on the machine. It thus remains to estimate the spindle dynamics from the given data. Depending on the design of the measurement device, different reconstruction methods can be employed.

2.2 Device layouts and reconstruction algorithms

In the presented approach, the excitation forces applied to the assembled spindle-device structure (i.e., the components of $F_{A,i}$) are generated by embedded axial piezoelectric actuators, and the assembly's responses are measured using accelerometers installed at multiple locations on the device.

As the actuators are embedded into the device, the effect of a single actuator is a pair of external forces of equal magnitude and opposite directions at its supports. The quantities that can be measured are the displacement vector $X_{A,i}$ and the vector of actuator input voltages $V_{A,i}$. Consequently, the measurable frequency response function (FRF) matrix H_m corresponds to $X_{A,i} = H_m V_{A,i} = H_{A,ii} T_{in} V_{A,i}$ where T_{in} maps n independent actuator voltages to $2n$ external force inputs. The derivation of T_{in} for a single piezoelectric axial actuator is further explained in Section 3, e.g., in Eq. 15. The measurements of the device then provide the following FRF matrix:

$$\begin{aligned} H_m = H_{A,ii} T_{in} &= H_{D,ii} T_{in} \\ &- H_{D,ic}(H_{D,cc} + H_{S,cc})^{-1} H_{D,ci} T_{in} \end{aligned} \tag{5}$$

The goal now is to reconstruct $H_{S,cc}$ based on the known dynamics of the assembly H_m and the device H_D. Equation 5 can be evaluated for any device, that fits the description of Eq. 2, as long as $(H_{D,cc} + H_{S,cc})$ is invertible, regardless of the number of excitation inputs and sensors or their locations. However, solving Eq. 5 in closed-form for $H_{S,cc}$ is only possible under certain conditions which are discussed in more detail in Section 2.2.2. A necessary condition is that the device offers equally many independent excitation inputs and

sensors as components in $\boldsymbol{F}_{S,c}$ and $\boldsymbol{X}_{S,c}$, respectively. Thus, if the spindle receptance is considered to be a two-by-two receptance matrix, the device needs to offer two independent excitation inputs and two independent response sensors.

Based on this, two device prototypes are developed that are described in the following two subsections: The first one (Section 2.2.1) is simple and compact but does not offer sufficiently many excitation inputs for a closed-form spindle receptance reconstruction. Instead, a spindle reconstruction method based on a modal model of the spindle and gradient-based optimization is proposed. In the remainder of the document, this device is referred to as "one-stage device." The other prototype (Section 2.2.2) is less compact but allows to use a closed-form spindle reconstruction approach. The term "two-stage device" shall refer to this device in the following.

2.2.1 One-stage device and optimization-based spindle receptance reconstruction

This prototype device is made from stainless steel and has the spindle interface of HSK A63 and the geometry shown in Fig. 2. It features a relatively compliant section in the middle, around which four axial piezoelectric actuators are arranged. Two opposing piezoelectric actuators are driven with voltages of equal magnitude and opposite polarity, hereby exciting bending modes of the structure. The device thus offers one independent excitation input for the X and one for the Y direction. To capture the dynamic response, six accelerometers—three in X and three in Y direction—are attached to the device.

A modal model according to [23] (Eq. 3.74 in this reference) is chosen to represent the spindle receptance matrix, as provided by the following:

$$H(s) = \sum_{k=1}^{m} \frac{\boldsymbol{u}_k \boldsymbol{u}_k^T}{s^2 + 2\zeta_k \omega_{n,k} s + \omega_{n,k}^2} \tag{6}$$

It assumes the linear behavior of the structure and inherently enforces the receptance matrix to be symmetric. Potential nonlinearities in the spindle receptance could be captured by making these modal parameters dependent on, e.g., static load or spindle speed, as is done by [24]. The number of modes m is a hyperparameter that needs to be determined in advance while the eigenfrequencies $\omega_{n,k}$, damping ratios ζ_k, and mass-normalized mode shapes u_k are the optimization parameters.

Based on this spindle receptance model and the calibrated dynamics of the device (see Section 3.1), Eq. 5 is evaluated, and the predicted response $\boldsymbol{H}_p$ is compared to actual measurements $\boldsymbol{H}_m$ at N frequency points ω_i through the following minimization loss function:

$$\begin{aligned} \mathscr{L}(\boldsymbol{H}_m, \boldsymbol{H}_P(\theta)) = {} & \frac{1}{N} \sum_{i=0}^{N} \left\| \log_{10}(|\boldsymbol{H}_m(\omega_i)|) - \log_{10}(|\boldsymbol{H}_P(\omega_i, \theta)|) \right\| \\ & + \gamma_1 \frac{1}{N} \sum_{i=0}^{N} \left\| \angle \boldsymbol{H}_m(\omega_i) - \angle \boldsymbol{H}_P(\omega_i, \theta) \right\| \\ & + \gamma_2 \sum_{k=0}^{m} (\max(0, -(\omega_k - \omega_{min})) \\ & + \max(0, \omega_k - \omega_{max})) \end{aligned} \tag{7}$$

with $|\boldsymbol{H}|$ and $\angle \boldsymbol{H}$ representing the element-wise magnitude and phase of complex-valued matrix elements, respectively. $\|\bullet\|$ also stands for Euclidean norm of matrices. In other words, the first two terms are the mean squared errors of the log magnitude and phase of the predicted and measured FRFs
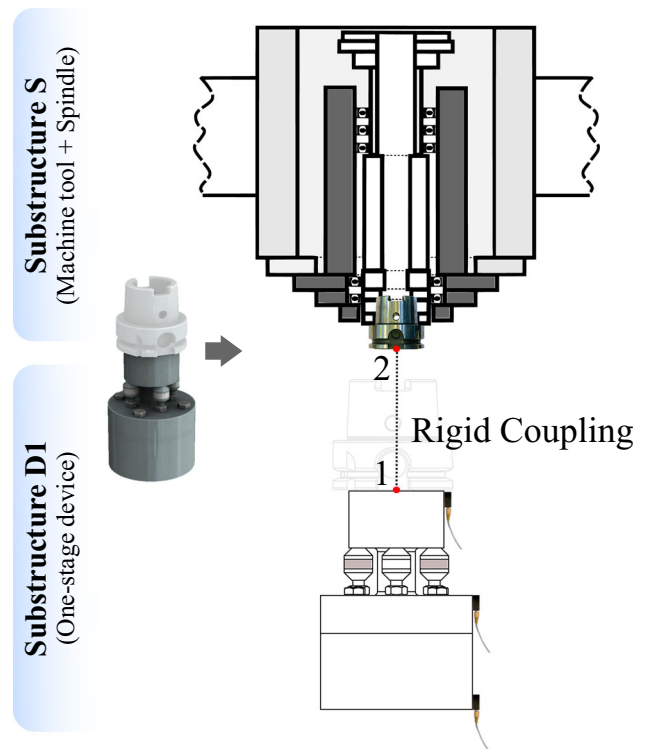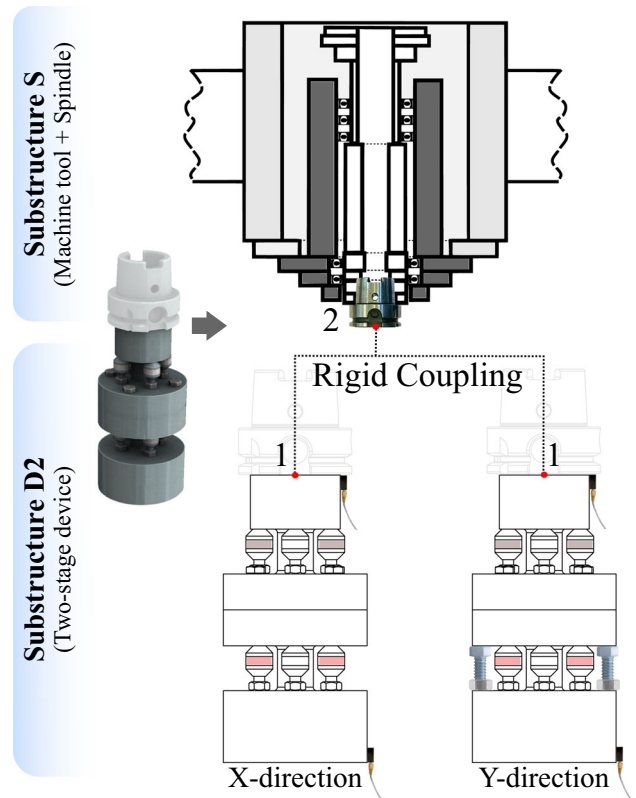

Fig. 2 Structural arrangement of the intended machine tool with the one-stage device. Highlighted piezoelectric actuators in gray are excited with opposite polarization to shake bending dynamics. Three indicated accelerometers are meant to measure the lateral response (X direction) of the machine tool-device assembly

Table 1 Overview of model parameters, reparametrization, and initialization

Model parameter	Reparametrization	Initialization
ω_n	$\omega_k = e^{p_{1,k}}$	$p_{1,k} = log(\omega_{min} + \frac{k}{m}(\omega_{max} - \omega_{min}))$
ζ_k	$\zeta_k = e^{p_{2,k}}$	$p_{2,k} = 0.01$
$u_{k,i}$	$u_{k,i} = e^{(p_{3,k,i} + jp_{4,k,i})}$	$p_{3,k,i} = p_{4,k,i} = 0.0$

ω_{min} and ω_{max} are the bounds of the considered frequency range. m is a hyperparameter that sets the number of modes

averaged over frequencies ω_i. The third term acts as a constraint and encourages the eigenfrequencies to stay within the meaningful frequency range of $(\omega_{min}, \omega_{max})$. $\boldsymbol{\theta}$ is the collection of optimization parameters, and γ_1 and γ_2 are hyperparameters to balance the loss terms.

For easier optimization, the model parameters are reparametrized using the natural logarithm (for eigenfrequencies and damping ratios). This not only enforces them to remain positive but also allows easier exploration, i.e., to find the suitable order of magnitude more quickly. Similarly, the elements of the mass-normalized mode shape u_k are expressed in terms of log magnitude and phase. An overview of optimization parameters and their reparametrizations and initializations is given in Table 1.

PyTorch [25] is used for the implementation of the spindle model, device model, and loss function which allows using its automatic differentiation functionality to obtain gradients of the loss function. The Adam optimizer [26] is employed to minimize the loss function using batch gradient descent.

2.2.2 Two-stage device and closed-form spindle receptance reconstruction

This device is made from stainless steel and has a spindle interface of HSK A63 similar to the one-stage device. However, at the cost of being less compact, the two-stage device features a second stage of piezoelectric actuators (Fig. 3). Again, two opposing piezoelectric actuators are driven with voltages of equal magnitude and opposite polarity.

The two stages of piezoelectric actuators offer two independent excitation inputs per X and Y directions. Consequently, a closed-form spindle dynamics reconstruction method can be used, which is described next. Solving Eq. 5 for $\boldsymbol{H}_{S,cc}$ yields the following:

$$\boldsymbol{H}_{S,cc} = \boldsymbol{H}_{D,ci}\boldsymbol{T}_{in}(\boldsymbol{H}_{D,ii}\boldsymbol{T}_{in} - \boldsymbol{H}_m)^{-1}\boldsymbol{H}_{D,ic} - \boldsymbol{H}_{D,cc} \quad (8)$$

As $\boldsymbol{H}_{S,cc}$ is expected to be symmetric, the off-diagonal components are averaged, i.e., $\boldsymbol{H}_{S,cc,sym} = 0.5(\boldsymbol{H}_{S,cc} + \boldsymbol{H}_{S,cc}^T)$. Equation 8 requires $(\boldsymbol{H}_{D,ii}\boldsymbol{T}_{in} - \boldsymbol{H}_m)$, $(\boldsymbol{H}_{D,ci}\boldsymbol{T}_{in})$, and $\boldsymbol{H}_{D,ic}$

Fig. 3 Structural arrangement of the intended machine tool with the two-stage device. Highlighted piezoelectric actuators in gray and light red provide two independent excitations to machine tool-device assembly while the indicated accelerometers record the resulting lateral response. The indicated jamming bolts in the Y direction are used to disturb symmetry in device dynamics in X and Y directions

to be invertible. The inverses of the latter two terms are required in solving for $\boldsymbol{H}_{S,cc}$. In words, the invertibility of $(\boldsymbol{H}_{D,ci}\boldsymbol{T}_{in})$ implies that the actuators embedded in the device need to be able to cause displacements in all DOFs of $\boldsymbol{X}_{D,c} = \boldsymbol{X}_{S,c}$. Thus, if $\boldsymbol{X}_{S,c} = [X, \theta_x]^T$, then two actuators are needed that cause two linearly independent displacement vectors at the coupling point. Similarly, the invertibility of $\boldsymbol{H}_{D,ic}$ requires that any force vector $\boldsymbol{F}_{D,c}$
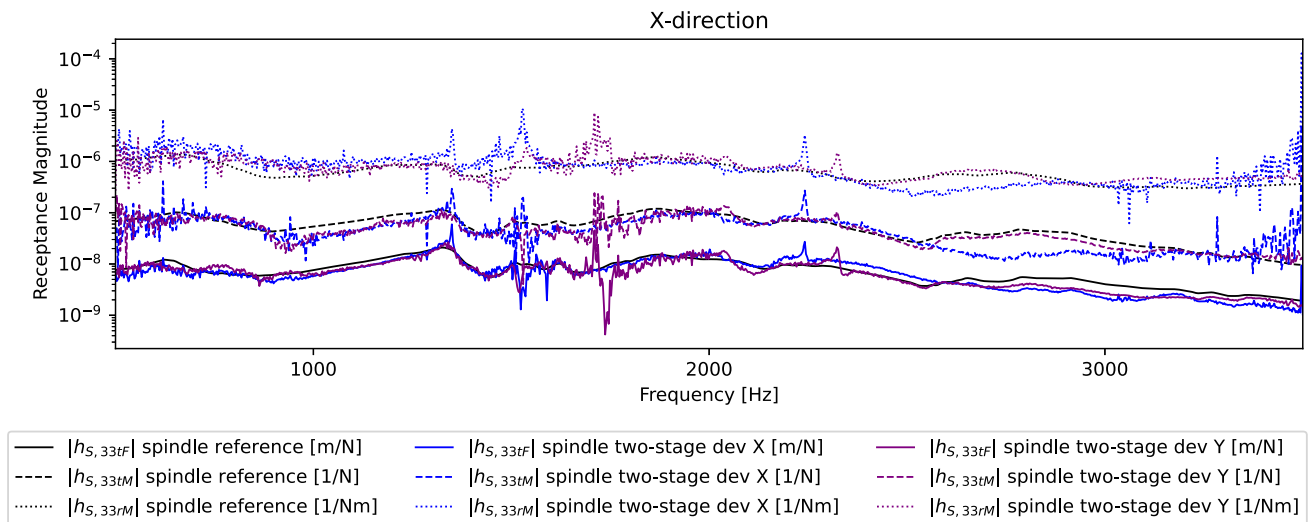
Fig. 4 Translational and rotational components of the spindle dynamics of a GFMS Mikron HPM800U 5-axis milling machine in X direction as estimated by the two-stage device in two different orientations and a reference obtained as suggested in [27]. In one case, the X-axis of the device was aligned with the X-axis of the machine while in the second case, the Y-axis of the device was aligned with the X-axis of the machine. The two predictions are corrupted around different frequencies (approximately 1500 Hz and 1700 Hz), because the dynamics of the two-stage device is different in X and Y directions

applied at the coupling point causes a unique displacement vector $X_{D,i}$ that can be captured by the embedded sensors. Hence, if $\boldsymbol{F}_{S,c} = -\boldsymbol{F}_{D,c}$, two sensors must be placed in different locations. Finally, the invertibility requirement of $(\boldsymbol{H}_{D,ii}\boldsymbol{T}_{in} - \boldsymbol{H}_m)$ means that the measurements obtained from the device when mounted to the spindle should be different from measurements obtained from substructure D (the device without HSK section) alone. Note that the above conditions must hold on a frequency-by-frequency basis in the frequency range of interest.

The spindle receptance estimates resulting from Eq. 8 are corrupted by inevitable model mismatch, which becomes particularly pronounced around eigenfrequencies of the device where the term that needs to be inverted may become ill-conditioned. Reconstruction errors can be reduced if the eigenfrequencies of the device are chosen to be outside the frequency range of interest or if the device model can be determined with extremely high accuracy. If neither of these requirements can be satisfied, a remaining solution is to repeat the spindle receptance measurement with two different device dynamics, i.e., different in terms of their eigenfrequencies. This approach is chosen to obtain accurate spindle receptance estimates with the available prototype. The device dynamics in the Y direction are altered by jamming a pair of bolts in the lower piezo stage, as shown in Fig. 3.

The measurement of the spindle receptance should be then performed once with the X-axis of the device aligned with the X-axis of the machine, and once with the Y-axis of the device aligned with the X-axis of the machine (i.e., a 90° rotation of the device between measurements). The same procedure should be carried out for measuring the Y-axis of the machine. This essentially yields two estimates of the spindle receptance from two different device dynamics (denoted $\boldsymbol{H}_{S,cc1,sym}$ and $\boldsymbol{H}_{S,cc2,sym}$) per direction. Consequently, the spindle receptance estimates obtained using Eq. 8 are corrupted around different frequencies, as can be seen in Fig. 4.

The FRF components of the two estimates are then combined by computing their weighted arithmetic mean. The weights for measurements 1 and 2 and are defined as

$$r_{1,ij}(\omega) = 1 - \frac{|\sigma_{1,ij}(\omega)|}{|\sigma_{1,ij}(\omega)| + |\sigma_{2,ij}(\omega)|}$$
$$r_{2,ij}(\omega) = 1 - \frac{|\sigma_{2,ij}(\omega)|}{|\sigma_{1,ij}(\omega)| + |\sigma_{2,ij}(\omega)|} \quad (9)$$

where $\sigma_{k,ij}(\omega)$ is the sliding window standard deviation (considering a window length of $2P + 1$ samples) of the FRF component ij of measurement k at frequency point ω_l computed as follows:

$$\sigma_{k,ij}(\omega_l) = \sqrt{\frac{1}{2P+1} \sum_{p=-P}^{P} (H_{k,ij}(\omega_{l+p}) - \bar{H}_{k,ij})^2} \quad (10)$$
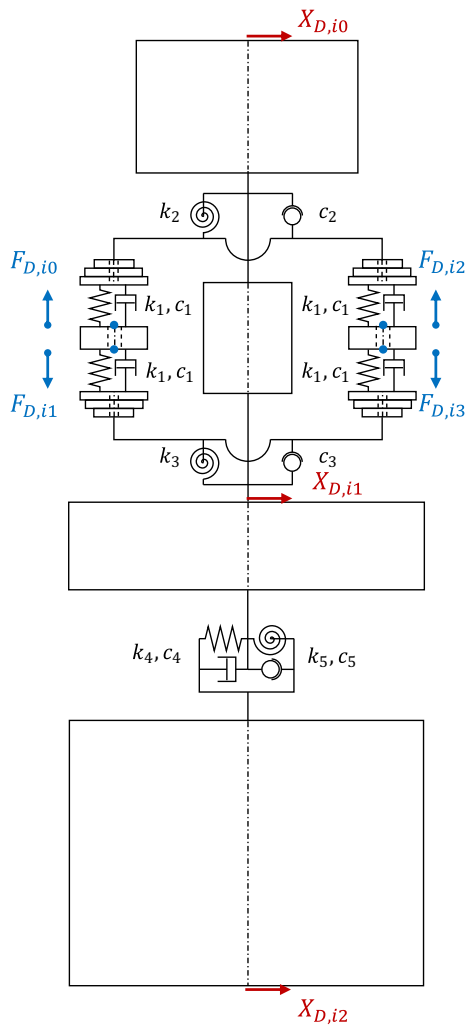
Fig. 5 Dynamics model of the one-stage device: Cylinders (drawn as rectangles) subject to lateral or axial load are assembled through rigid and elastic receptance coupling. External force inputs (blue) model the piezoelectric effect of the applied voltage. Displacement outputs are denoted in red

Before computing the weighted average, the two measurements are smoothed using moving median filtering on magnitude and phase. Finally, the resulting spindle receptance is computed as $H_{S,cc,av,ij} = r_{1,ij} H_{S,cc1,sym,ij} + r_{2,ij} H_{S,cc2,sym,ij}$. The FRFs of the device are obtained as described in Section 3.2.

3 Bending dynamics of the measurement devices

This section is devoted to obtaining the required dynamics of the two device configurations as they are involved in the coupled machine tool-device dynamic behavior according to Eq. 4.

Due to the design of the prototype devices described in Sections 2.2.1 and 2.2.2, its lateral dynamics in X and Y directions are expected to be independent of each other (i.e., no axis cross-coupling). The models of the device dynamics presented in the following are thus restricted to uni-directional translational and rotational deformations. The HSK-A63 interface is not part of the device models, as it is considered to be part of the machine tool.

In Section 3.1, it is suggested that utilizing a simplified Timoshenko beam model could yield an adequately precise model for the one-stage device and optimization-based spindle receptance reconstruction approach. The two-stage device, on the other hand, involves more components and complexities, and hence, developing a physics-based device model through modeling and calibration could be an extensive task. To provide an alternative solution, Section 3.2 presents an experimental approach based on inverse RCSA for obtaining device models.

3.1 Physics-based modeling and calibration

The receptance of the one-stage prototype device is modeled through sequential receptance coupling of cylinders under axial or lateral load, as detailed in Section 3.1.2. The Timoshenko beam model is used to compute the receptance of a single cylinder subject to lateral forces and bending moments at its ends. For the axial receptance of a uniform rod, the analytical solutions provided in [28] are used. The cylindrical piezoelectric axial actuators embedded in the device are modeled as mere elastic structures. The converse piezoelectric effect is modeled by a pair of external forces as described in Section 3.1.1, following the approach taken in [29].

3.1.1 Piezoelectric actuator

Let the axial receptance of a linear elastic rod be given through the following receptance matrix:

$$\begin{bmatrix} Z_1 \\ Z_2 \end{bmatrix} = \begin{bmatrix} H_{11} & H_{12} \\ H_{21} & H_{22} \end{bmatrix} \begin{bmatrix} F_{z1} \\ F_{z2} \end{bmatrix} \tag{11}$$

The elongation of a piezoelectric material due to the voltage V applied across its end faces can be described by

$$Z_2 - Z_1 = \begin{bmatrix} H_{21} - H_{11} & H_{22} - H_{12} \end{bmatrix} \begin{bmatrix} F_{z1} \\ F_{z2} \end{bmatrix} + d_{33} V \tag{12}$$

where the force-induced portion of the deformation is based on the axial receptance according to Eq. 11 and d_{33} is the piezoelectric coefficient. The voltage-induced portion of the elongation is now replaced by a pair of external forces of equal magnitude F_{ext} and opposite directions:

$$Z_2 - Z_1 = \begin{bmatrix} H_{21} - H_{11} & H_{22} - H_{12} \end{bmatrix} \begin{bmatrix} F_{z1} + F_{ext} \\ F_{z2} - F_{ext} \end{bmatrix} \quad (13)$$

Comparing the above two equations yields an expression for the magnitude of the external force in terms of applied voltage and receptance of the piezoelectric material:

$$F_{ext} = \frac{d_{33}V}{H_{21} + H_{12} - H_{11} - H_{22}} \quad (14)$$

The mapping from actuator inputs (a single excitation voltage in this case) to external forces reads as follows:

$$\begin{bmatrix} F_{z1,ext} \\ F_{z2,ext} \end{bmatrix} = \boldsymbol{T}_{in}V = \begin{bmatrix} 1 \\ -1 \end{bmatrix} \frac{d_{33}}{H_{21} + H_{12} - H_{11} - H_{22}}V \quad (15)$$

3.1.2 Assembled model through coupling substructures

An overview of the dynamics models of the one-stage device is given in Fig. 5. The cylinders are drawn as rectangles; their center axes as dash-dotted lines. Solid lines denote rigid couplings whereas linear and rotational elastic couplings are indicated by the respective pictograms. The latter has been introduced between the piezoelectric elements and the neighboring components (k_1, c_1). They are supposed to model the effect of the 0.1 mm thin copper electrodes and a 0.07-mm thin plastic insulation sheet which are found in these locations in the physical prototype. Axial forces and displacements at the ends of the two piezo stacks are mapped to moments and rotational displacements through linear mapping.

Elastic couplings are further introduced between this assembly of piezo stacks and the surrounding frame (k_2, c_2 and k_3, c_3). They should take into account any local deformations and contact stiffnesses. Finally, linear and rotational spring-damper systems are introduced where the physical device is bolted together (k_4, c_4, k_5, c_5). The free inputs and outputs of the device model are indicated in blue and red, respectively. For the one-stage device, they correspond to $\boldsymbol{F}_{D,i}$ and $\boldsymbol{X}_{D,i}$ from Eq. 2 as follows:

$$\boldsymbol{F}_{D,i} = \begin{bmatrix} F_{D,i0} & F_{D,i1} & F_{D,i2} & F_{D,i3} \end{bmatrix}^T \quad (16)$$

$$\boldsymbol{X}_{D,i} = \begin{bmatrix} X_{D,i0} & X_{D,i1} & X_{D,i2} \end{bmatrix}^T \quad (17)$$

3.1.3 Model calibration

To capture the dynamics of the device alone (i.e., not attached to any machine tool), it is hung from an elastic string to simulate free-free boundary conditions. FRF measurements are then obtained from the actuators and sensors embedded in the device as well as from tap testing on two points on the tool-holder part.

A Timoshenko beam-based model of the tool-holder taper is added to the device model through receptance coupling, as it is considered to be part of the machine tool and is thus not included in the device model. The device model is then calibrated by tuning model parameters using genetic algorithm optimization, such that the obtained measurements match the FRFs predicted by the device model. All of the aforementioned contact parameters (k_i, c_i) as well as the outer diameter and Young's modulus of the center bolt are considered optimization parameters. The properties of the center bolt are tuned to take the effect of the two/four piezo stacks into account which is not considered in this planar model.

3.2 Experimental modeling through inverse RCSA

This approach aims to obtain all required components of the device FRFs through measurements. The obstacle here is applying rotational moments at the coupling point with the spindle, which is not practical in reality. To circumvent this issue, the top part of the device is modeled using a Timoshenko beam model and is considered known. The FRF measurements are taken from the device in free-free condition using the embedded actuators and sensors on the unknown part of the device, as well as through impacting and measuring on the known part of the device (Fig. 7). The FRFs of the unknown part of the device can then be obtained using inverse RCSA. Finally, part of the subtracted structure is added again to get the model of the device up to the desired coupling location. A graphical overview of the method is given in Fig. 6.

For obtaining the measurements, the device was again hung from an elastic string to simulate free-free boundary conditions, as shown in Fig. 7.

4 Experimental validations

The two versions of the measurement device are used to estimate the spindle receptance of a GFMS Mikron HPM800U 5-axis milling machine in the setup shown in Fig. 8. An exponential chirp excitation ranging from approximately 80 Hz to 6 kHz with a voltage amplitude slightly below 100 V is used for both devices. The excitation and response
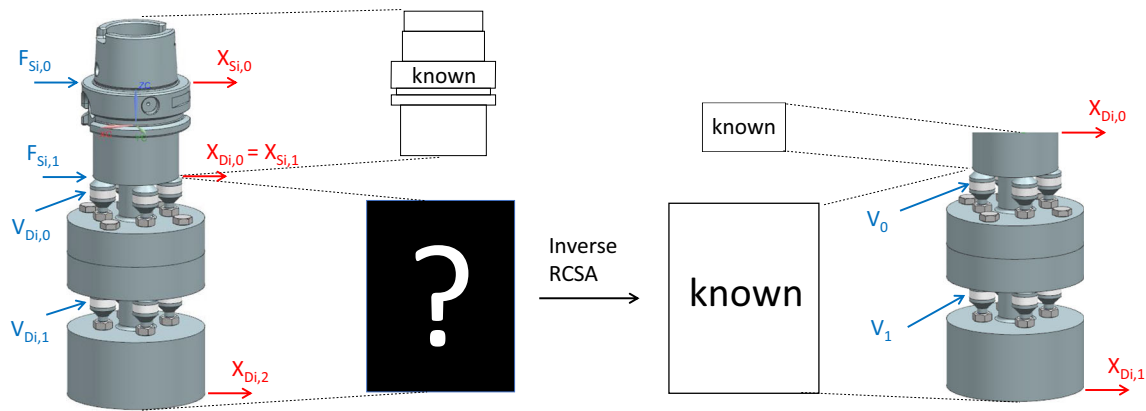
Fig. 6 Device dynamics identification method based on inverse RCSA, where the FRFs of unknown substructures are determined by subtracting theoretical models of known parts from the measurements of the intact device

signals are sampled at 51.2 kHz using a National Instruments data acquisition card type 9234. PCB Piezotronics accelerometers of type 352C22 are employed to capture the response. The measurements are repeated 100 times to average out measurement noise. The number of modes of the modal spindle model used with the one-stage device and the optimization-based spindle receptance reconstruction is chosen to be $m = 10$ as a hyperparameter. The resulting modal parameters can be found in Appendix A. For the two-stage device, measurements are conducted as multiple SIMO (single input multi output) experiments, using one excitation input at a time and setting the other voltage input to zero by short-circuiting the electrodes of the piezoelectric actuators.

4.1 Validations of estimated spindle dynamics versus manual impact testing

The estimated spindle dynamics by the two device layouts are compared against reference values in Fig. 9. The reference receptance is obtained through an inverse receptance coupling approach as suggested by Namazi et al. [27]. In this method, a cylindrical dummy holder is mounted to the machine, and FRFs are measured at certain locations through impact testing. This indirect measurement method is proposed since the excitation of rotational dynamics by a hammer is not straightforward. In the following, the measurements of the machine's dynamics at the spindle flange are compared against each other.

4.2 Validations through tooltip dynamics

As mentioned earlier, the structural dynamics at the tooltip determine the boundaries of stable process conditions. Hence, it is valuable to evaluate the validity of the reconstructed spindle dynamics from the proposed devices by comparing

the resulting tooltip dynamics using RCSA to impact testing measurements. Seven different tool-holder combinations
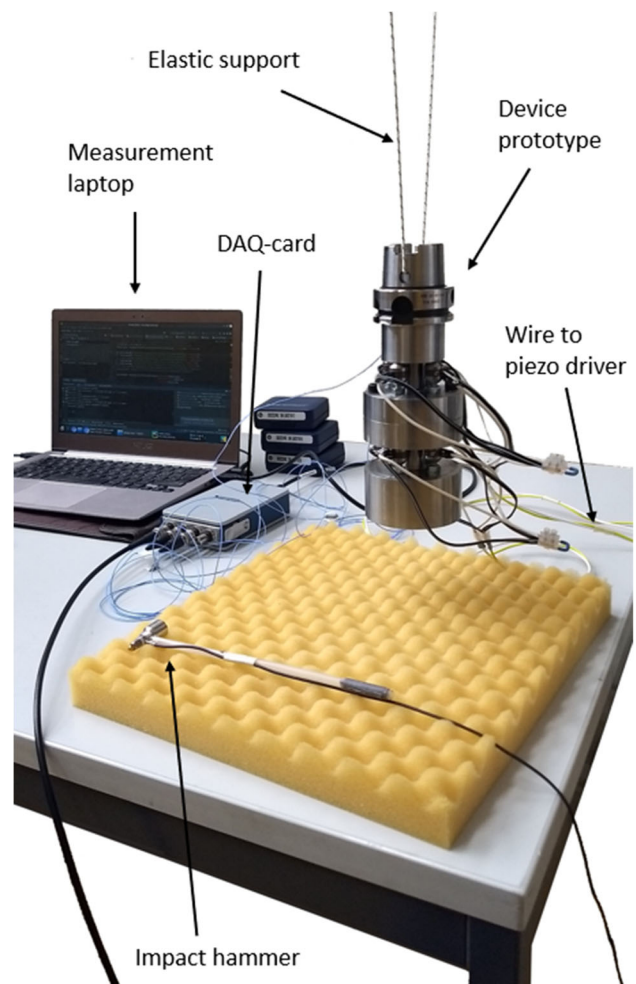
Fig. 7 The two-stage device during structural identification. To simulate free-free boundary conditions, it is hung from an elastic string

Fig. 8 The prototype devices mounted to a GFMS Mikron HPM800U 5-axis machining center. Left: one-stage device. Right: two-stage device
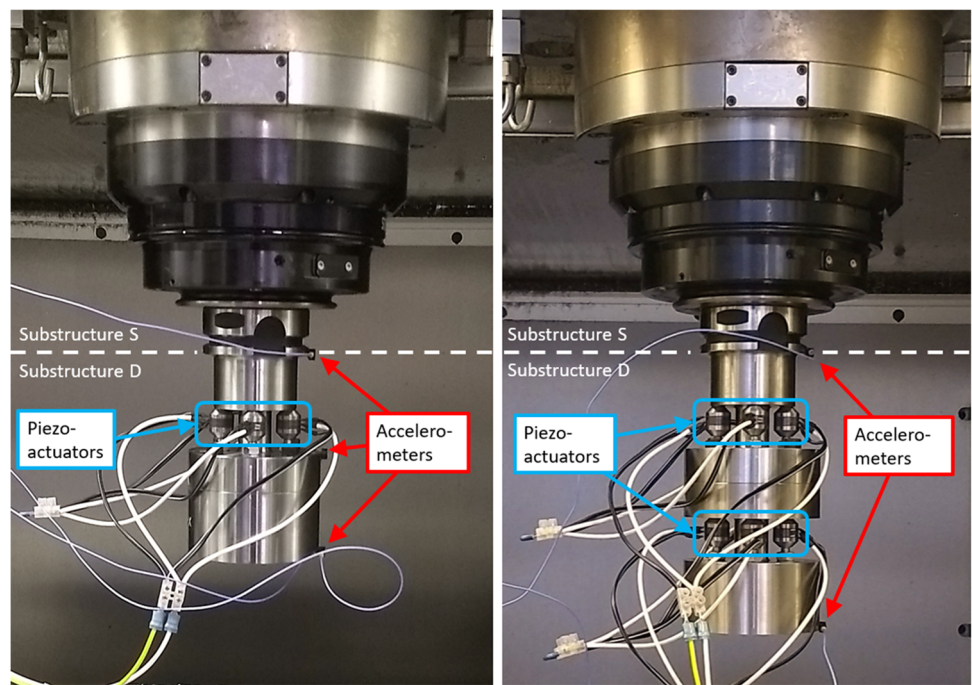
are selected for this validation purpose. The details of these combinations are provided in Table 2. The dynamics of the tooling systems are obtained through a finite element modeling approach based on Timoshenko beam elements with considering a non-uniformly distributed contact flexibility at the tool-holder interface. More details and corresponding values of the contact parameters can be found in [13].

Considering the substructuring scenario presented in Fig. 10 with $X_{T,2} = X_{S,3}$ and $F_{T,2} + F_{S,3} = \mathbf{0}$ as compatibility and equilibrium conditions respectively, the coupled dynamics of the system at the tooltip can be computed as follows:

$$H_{ST,11} = H_{T,11} - H_{T,12}(H_{S,33} + H_{T,22})^{-1} H_{T,21} \qquad (18)$$

Further details of substructure coupling through the RCSA method can be found in publications of Schmitz et al. [30, 31].
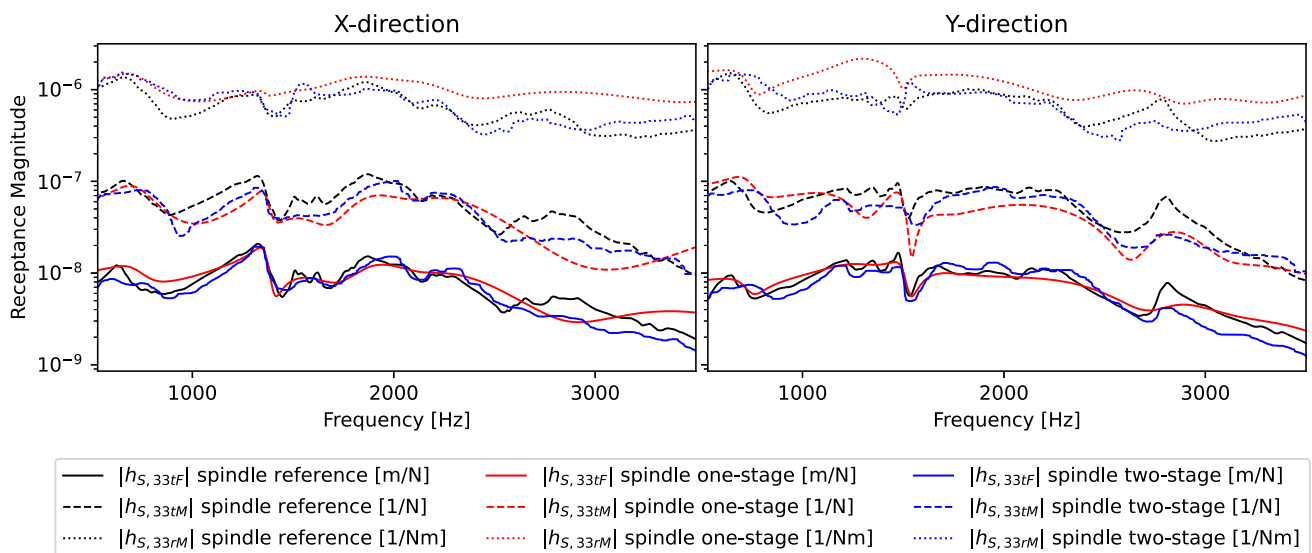
Fig. 9 Translational and rotational components of the spindle dynamics of a GFMS Mikron HPM800U 5-axis milling machine in *X* and *Y* directions as estimated by the one-stage device, the two-stage device, and the reference obtained through iRCSA

Table 2 Tooling systems (S.L. indicates the stickout length of the cutting tool)

#	Holder	Tool	S.L. (mm)	Picture
1	Zürn HSK-A63 63.11.20.2 Interface: Collet ER32	Voha 12032456120 4 flutes	70.50	
2	REGO-FIX PG25x100H Interface: powRgrip PG25	Diameter: 12.0 mm Length: 110.5 mm	65.90	
3	REGO-FIX PG25x100H Interface: powRgrip PG25		60.90	
4	Schunk 208123 50161717 Interface: Thermal shrink fit		62.60	
5	Zürn HSK-A63 11.16.23 Interface: Collet ER25	Voha 2002805 4 flutes Diameter: 16.0 mm Length: 93.3 mm	60.07	
6	Long insert tool	5 cutters Diameter: 40.0 mm	–	
7	Short insert tool	5 cutters Diameter: 50.0 mm	–	

Figure 11 shows tooltip receptance measurements for the tool-holder combinations described in Table 2 along with the predictions using on the spindle receptance measurements from the one-stage device, the two-stage device, and the reference dynamics through iRCSA.

Fig. 10 Coupling scenario of the machine tool structure and tooling system. The model for tooling systems is obtained from the method presented in [13]

4.3 Validations of predicted stability boundaries against experimental observations

Experimental observations of stability states and corresponding chatter frequencies are used to verify the model-based prediction of SLDs through the zero-order approximation method by Altintas and Budak [3]. The required tooltip dynamics are taken from the RCSA coupling presented in the preceding section. The validation cuts are collected through experimental cutting tests for the first two tool-holder combinations from Table 2 on a block of Al6082 aluminum. Table 3 summarizes the corresponding process parameters. In the prediction of stability charts, the experimentally calibrated values of 902 MPa and 243 MPa are assumed for the tangential and radial cutting force coefficient, respectively.

An acceptable overall agreement between the three predictions and the validation data can be observed for the first validation case in Fig. 12a. In the second case (Fig. 12b), the predictions based on the reference spindle receptance and the estimate from the two-stage device are in agreement, but the predicted critical depth of cut based on the spindle receptance estimate from the one-stage device is slightly higher. This is due to an inaccuracy in the magnitude of the corresponding tooltip receptance in Y direction (Fig. 11b), which is underestimated for frequencies around the dominant mode (2100–2300 Hz). It is worth noting that the SLDs generated using the measured tooltip FRFs show slight deviations from those produced by the predicted FRFs. However, this deviation is not necessarily positive in terms of improved prediction accuracy of the stability borders ver-
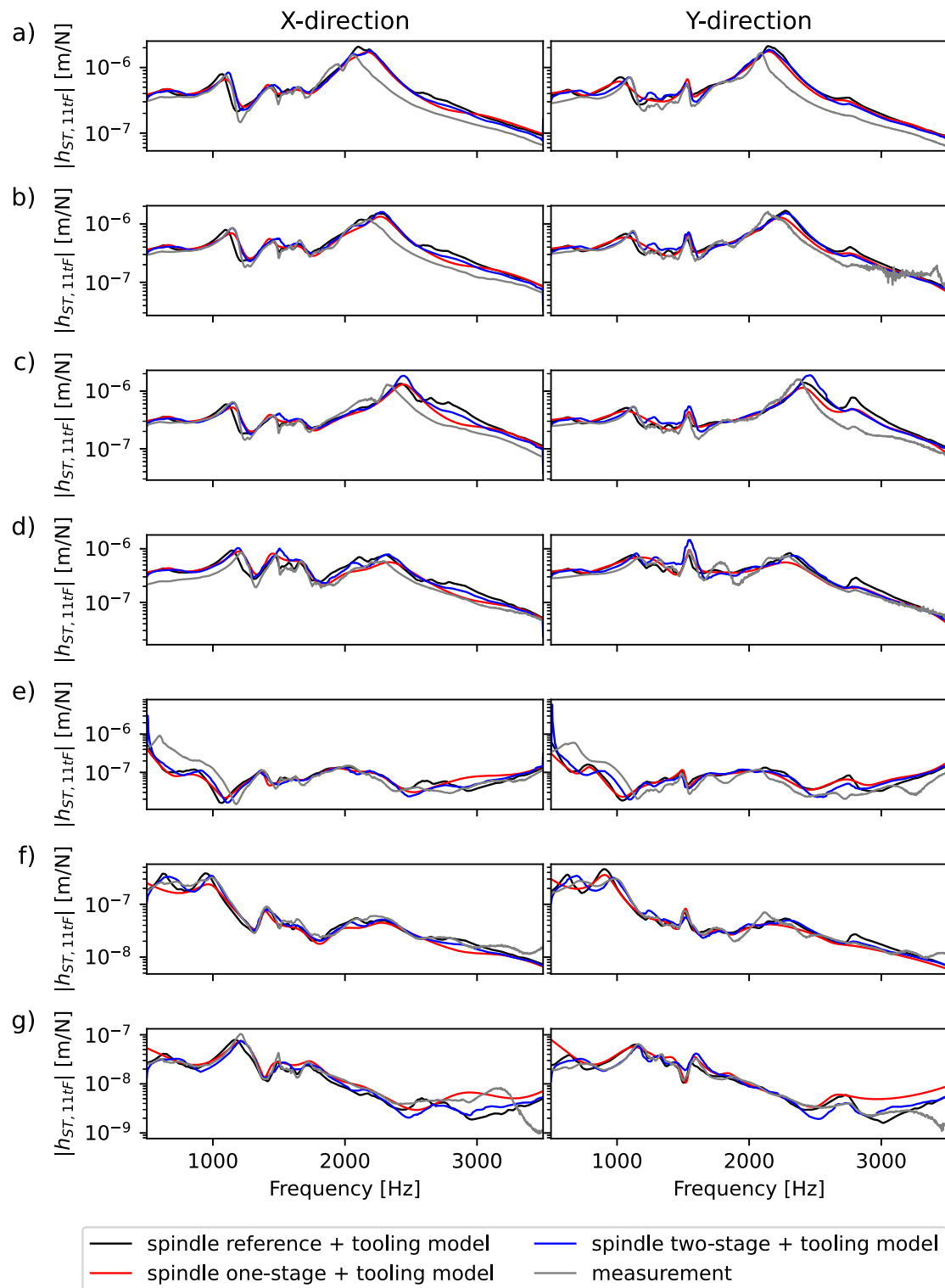
Fig. 11 Tooltip receptance predictions and measurement for tool-holder combinations #1 to #7 in Table 2 correspond to **a** to **g**, respectively. Predictions are based on spindle receptance estimations from the one-stage device, two-stage device, and a reference obtained using the method presented in [27]. These spindle receptances are rigidly coupled with Timoshenko-beam-based tooling models to obtain tooltip predictions

Table 3 Process parameters used for the validation cuts with two tool-holder combinations (according to Table 2) on a block of Al6082 aluminum

Case	Tooling system	Feed direction	Milling Strategy	Radial depth of cut (mm)	Feed rate (mm/tooth)
1	1	$Y+$	Slotting	12.0	0.05
2	2	$X+$	Up-milling	8.4	0.05

sus the validation cuts. This raises the possibility that the direct measurement of tooltip FRFs using an impact hammer and accelerometer may be compromised. The imprecision may stem from misalignment in the direction and location of hammer impacts or the accelerometer, particularly given the fluted geometry of the tooltip.

5 Conclusion

This study introduced two prototypes of measurement devices and their identification methods to automatically identify machine tool dynamics at the spindle interface. The two devices differ in the number of independent piezoelectric actuators and embedded acceleration sensors, as well as in their compactness. Both approaches produced satisfactory results.

The estimation of spindle dynamics using the one-stage device provides a compact measurement system with acceptable measurement accuracy. In the underlying optimization-based reconstruction method, like any optimization problem, attention must be given to the convergence to local minimums, such as when translational and rotational FRFs compensate for each other. Further inclusion of physical constraints or prior knowledge can be helpful for the convergence of the optimization to global solutions.

The two-stage device and the closed-form reconstruction method for spindle receptance estimation led to faster, unique, and repeatable results. However, the device compactness is compromised due to the additional stage of piezoelectric actuators. Future work could explore a more sophisticated arrangement of piezoelectric actuators, such as the Stewart-platform arrangement [32], which offers independent excitation inputs while maintaining a compact design. Improving the accuracy of the device model can further enhance the precision of the reconstructed spindle dynamics, which encourages arrangements that can be more reliably modeled in the design stage.

The two proposed measurement devices enabled the identification of machine tool receptance with high repeatability and minimal human effort, as only mounting the device on the machine tool is required. Additionally, the approach is suitable for measuring the machine tool dynamics in various locations in the working space since the device can be easily moved around without requiring external support. Further-more, the spindle receptance reconstruction method could be expanded to capture axis cross-couplings, which involves the response of the spindle in the X direction to the excitation in the Y direction and vice versa.
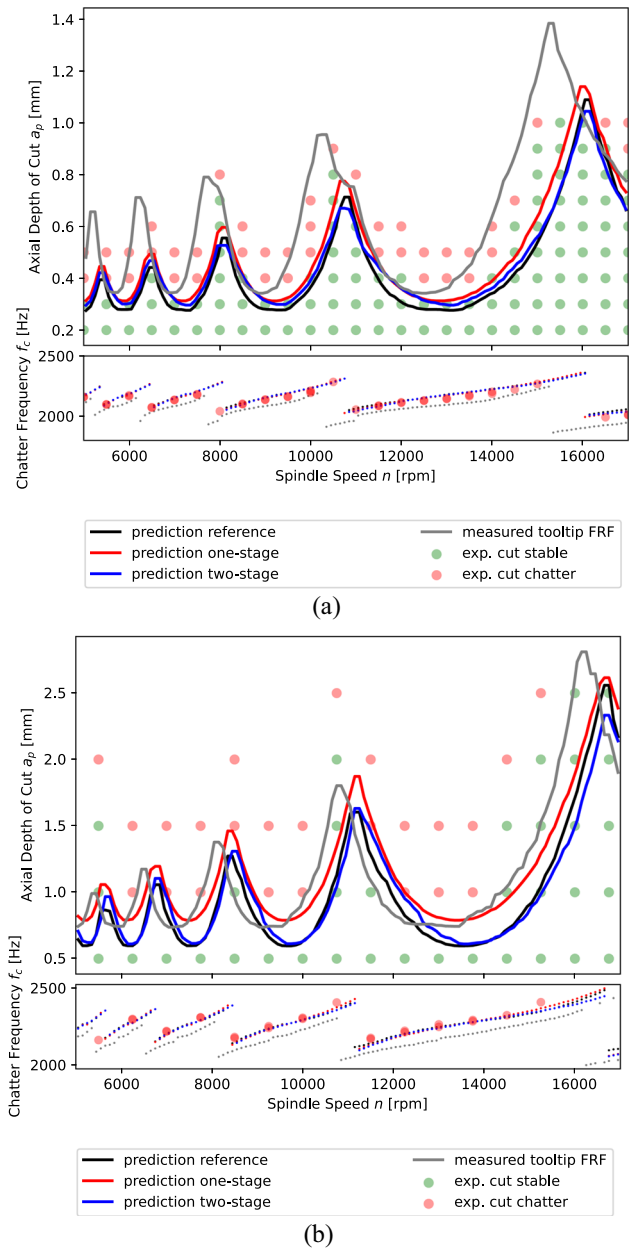
Fig. 12 Predicted stability boundaries and experimental chatter observations for tool-holder combination #1 in **a** and #2 in **b** from Table 2 using process parameters according to Table 3 on a block of Al6082 aluminum

Appendix A: Modal parameters of estimated spindle receptances

Table 4 Modal parameters of the spindle receptance in *X* direction as estimated by the one-stage device and optimization-based identification method

k	$\omega_{n,k}\ [rad/s]$	$\zeta_k\ [-]$	$u_{k,0}\ [\sqrt{s/kg}]$	$u_{k,1}\ [rad\sqrt{s/kgm^2}]$
1	1924.67	0.003	0.01134−0.00145j	−0.0271+0.0310j
2	4518.64	0.163	0.17878+0.025827j	1.9041+0.89598j
3	8562.86	0.028	0.23317−0.079048j	0.80471−0.085383j
4	9125.85	0.461	0.14483−0.72793j	2.7327−9.7517j
5	10,890.80	0.165	0.67985−0.64180j	2.2236−6.5233j
6	12,421.76	0.131	1.0155−0.10138j	5.3805−4.5614j
7	14,057.43	0.155	1.0305+0.35473j	9.6915−3.0552j
8	21,090.84	0.231	0.96087+0.61073j	0.31771+0.63735j
9	22,391.05	0.548	1.3746+1.3535j	36.942+10.874j
10	22,808.70	0.224	−0.849+0.97204j	−3.3365+18.436j

Table 5 Modal parameters of the spindle receptance in *Y* direction as estimated by the one-stage device and optimization-based identification method

k	$\omega_{n,k}\ [rad/s]$	$\zeta_k\ [-]$	$u_{k,0}\ [\sqrt{s/kg}]$	$u_{k,1}\ [rad\sqrt{s/kgm^2}]$
1	2239.41	0.113	0.03061−0.044494j	0.0235+0.00492j
2	4584.90	0.111	0.1209−0.03875j	1.8830−0.32124j
3	8107.34	0.141	0.29544+0.0776j	−2.9079−3.5816j
4	9437.61	0.031	0.1990−0.09720j	0.8738−1.8657j
5	10,271.24	0.109	0.28643+0.1873j	0.9037−2.8547j
6	15,633.82	0.251	1.2377−0.46629j	8.3055−0.17174j
7	17,837.63	0.079	0.43768+0.15219j	4.8724−5.0213j
8	20,598.82	0.162	0.7702+0.12895j	0.11743−13.038j
9	21,461.37	0.441	0.75704+1.3509j	36.08+15.436j
10	23,434.09	0.023	0.2007+0.042563j	0.20581+0.29781j

Declarations

Conflict of interest The authors declare no competing interests.

References

Publisher's Note Springer Nature remains neutral with regard to jurisdictional claims in published maps and institutional affiliations.